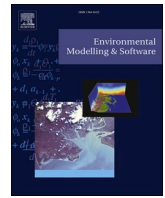




Contents lists available at ScienceDirect

# Environmental Modelling and Software

journal homepage: [www.elsevier.com/locate/envsoft](http://www.elsevier.com/locate/envsoft)

## Spatial prediction of air pollution levels using a hierarchical Bayesian spatiotemporal model in Catalonia, Spain

Marc Saez<sup>a,b</sup>, Maria A. Barceló<sup>a,b,\*</sup>

<sup>a</sup> Research Group on Statistics, Econometrics and Health (GRECS), University of Girona, Girona, Spain

<sup>b</sup> CIBER of Epidemiology and Public Health (CIBERESP), Madrid, Spain

### ARTICLE INFO

#### Keywords:

Spatial predictions  
Hierarchical Bayesian spatiotemporal model  
Stochastic partial differential equations (SPDE)  
Integrated nested laplace approximations (INLA)

### ABSTRACT

Our objective in this work was to present a hierarchical Bayesian spatiotemporal model that allowed us to make spatial predictions of air pollution levels effectively and with very few computational costs.

We specified a hierarchical spatiotemporal model using the Stochastic Partial Differential Equations of the integrated nested Laplace approximations approximation. This approach allowed us to spatially predict in the territory of Catalonia (Spain) the levels of the four pollutants for which there is the most evidence of an adverse health effect.

Our model allowed us to make fairly accurate spatial predictions of both long-term and short-term exposure to air pollutants with a relatively low density of monitoring stations and at a much lower computation time. The only requirements of our method are the minimum number of stations distributed throughout the territory where the predictions are to be made, and that the spatial and temporal dimensions are either independent or separable.

### 1. Introduction

In studies assessing the health effects of exposure to air pollution, there is the problem of how to estimate that exposure. Air pollution monitoring station locations do not usually coincide with where the majority of the subjects exposed to such pollution are found. In fact, the air pollution monitoring stations are not often distributed homogeneously in the territory under study, and it is quite usual that large areas, even some densely populated ones, do not have any stations at all.

Many studies use the measurements observed in the geographical region of the study to estimate, by means of point estimators, the exposure levels for that entire region. The estimators most widely used are the inverse-distance weighted average and the arithmetic mean of the values of the air pollutant observed in several monitoring stations, although sometimes the values of the pollutants observed in the nearest monitoring station are also used as estimators. The problem, as Wannemuehler et al. (2009) pointed out, is that when air pollution levels exhibit spatial variation across the study region, using these point estimators leads to a bias as a consequence of ignoring the spatial structure (i.e., spatial dependence) of the data. Furthermore, when that biased

estimated level is related to a health variable, this leads to an underestimation of the health effect of interest (Wannemuehler et al., 2009).

While there are numerous studies that propose models to estimate the levels of air pollutants, explicitly incorporating both spatial and temporal dependence (Cameletti et al., 2011, 2013; Pirani et al., 2013; Shaddick et al., 2013; Liang et al., 2015, 2016; Calculli et al., 2015; Cheam et al., 2017; Mukhopadhyay and Sahu, 2018; Chen et al., 2018; Clifford et al., 2019; Nicolis et al., 2019; Wan et al., 2021) (to refer to only some of those that have appeared in the last ten years), there are, however, fewer studies that attempt to predict air pollution levels in locations where there is no monitoring station (i.e., spatial prediction) and even fewer that evaluate the predictive capacity of the models they propose. With no intention of supplying an exhaustive list, among them we will cite the studies of Cameletti et al. (2011, 2013); Pirani et al. (2013); Shaddick et al. (2013); Mukhopadhyay and Sahu (2018); Nicolis et al. (2019), Wan et al. (2021) and Fiovaranti et al. (2021).

The spatial domain of these studies ranges from cities (Santiago de Chile - Nicolis et al., 2019; Beijing - Wan et al., 2021-) to countries (EU-15 countries - Shaddick et al., 2013; - Italy - Fiovaranti et al., 2021-), through to metropolitan areas (Greater London - Pirani et al., 2013-) and

\* Corresponding author. Research Group on Statistics, Econometrics and Health (GRECS) and CIBER of Epidemiology and Public Health (CIBERESP) University of Girona Carrer de la Universitat de Girona 10, Campus de Montilivi, 17003, Girona, Spain.

E-mail address: [antonia.barcelo@udg.edu](mailto:antonia.barcelo@udg.edu) (M.A. Barceló).

URL: <http://www.udg.edu/grecs.htm> (M.A. Barceló).

<https://doi.org/10.1016/j.envsoft.2022.105369>

Received 20 September 2021; Received in revised form 23 February 2022; Accepted 4 March 2022

Available online 10 March 2022

1364-8152/© 2022 The Authors. Published by Elsevier Ltd. This is an open access article under the CC BY-NC-ND license (<http://creativecommons.org/licenses/by-nc-nd/4.0/>).

regions (Po valley, northern Italy - Cameletti et al., 2011, 2013-; England and Wales - Mukhopadhyay and Sahu, 2018-). The pollutants that are predicted in these studies are coarse particles,  $PM_{10}$ , with a diameter of 10  $\mu m$  ( $\mu m$ ) or less (Cameletti et al., 2011, 2013; Pirani et al., 2013; Mukhopadhyay and Sahu, 2018; Fiovaranti et al., 2021), fine particles,  $PM_{2.5}$ , with a diameter of 2.5  $\mu m$  or less (Mukhopadhyay and Sahu, 2018; Nicolis et al., 2019; Wan et al., 2021), nitrogen dioxide,  $NO_2$  (Shaddick et al., 2013; Mukhopadhyay and Sahu, 2018) and ozone,  $O_3$  (Mukhopadhyay and Sahu, 2018). Regarding the frequency at which pollutants are observed, daily data (Cameletti et al., 2011, 2013; Pirani et al., 2013; Mukhopadhyay and Sahu, 2018; Fiovaranti et al., 2021) dominate, although hourly data (Nicolis et al., 2019; Wan et al., 2021) and annual data (Shaddick et al., 2013) are also used.

The models used in most of these articles, in addition to incorporating spatial and temporal dependencies, include explanatory variables among which appear, in decreasing order of the number of studies, meteorological variables (Cameletti et al., 2011, 2013; Pirani et al., 2013; Shaddick et al., 2013; Nicolis et al., 2019; Wan et al., 2021; Fiovaranti et al., 2021), other pollutants different from the one predicted (Cameletti et al., 2011, 2013), topographical variables (altitude - Cameletti et al., 2013; Wan et al., 2021- and distances to sea and roads - Shaddick et al., 2013; Fiovaranti et al., 2021 -, and to mountains - Wan et al., 2021-), site types (Pirani et al., 2013; Mukhopadhyay and Sahu, 2018), and land use variables (Shaddick et al., 2013).

With one exception (Wan et al., 2021), the studies use a Bayesian approach because it is the one that best allows the uncertainty of complex space-time data to be incorporated. Most of the studies that use the Bayesian approach perform the inference using the Monte Carlo Markov Chain (MCMC) (Cameletti et al., 2011; Pirani et al., 2013; Shaddick et al., 2013; Mukhopadhyay and Sahu, 2018; Nicolis et al., 2019). Only two use the Stochastic Partial Differential Equations (SPDE) representation of the INLA approximation (Cameletti et al., 2013; Fiovaranti et al., 2021). Using MCMC implies a high computational model complexity that, in some cases, prevents the practical application of the methods proposed by these studies. As an exception, it is worth mentioning Nicolis et al. (2019), who use the *spTimer* package (Bakar and Sahu, 2015). This package, which uses MCMC, allows large space-time data sets to be handled with fast computation and very good data processing capacity. The INLA approach is much more computationally effective than MCMC, producing accurate approximations to posterior distributions, even for very complex models (Lindgren and Rue, 2015).

These few studies that provide methods for spatial prediction use a relatively large number of monitoring stations. In this study, however, we intend to present an equally effective model that allows the use of information from a small number of monitoring stations. Furthermore, we intend to make spatial predictions at a much lower computational cost than existing methods. In fact, we consider that our contributions do consist of providing a method that allows spatial predictions to be made in territories with a low density of monitoring stations and with a much shorter computational time than other alternative methods.

Specifically, our objective in this work was to present a hierarchical Bayesian spatiotemporal model that allowed us to make effective spatial predictions of air pollution levels with very few computational costs. In this work, we used the SPDE representation of the INLA approximation to spatially predict, in the territory of Catalonia (Spain), the levels of the four pollutants for which there is the most evidence of an adverse health effect:  $PM_{10}$ ,  $NO_2$ ,  $O_3$  and  $PM_{2.5}$ . We performed the spatial predictions at a point level (defined by its UTM coordinates), allowing them to be aggregated later into any spatial unit required. We were especially interested in the long-term exposure to air pollutants. That is, by living in a certain area an individual is exposed to a mix of pollutants that have lasting effects on their health. We also considered the performance of our method to spatially predict short-term exposure to air pollutants, which has more temporary effects on health.

## 2. Methods

### 2.1. Data

We obtained information on the hourly levels of air pollution for 2011–2020 from the 143 monitoring stations from the Catalan Network for Pollution Control and Prevention (XVPCA) (open data) (Departament de Territori i Sostenibilitat, Generalitat de Catalunya, 2021), located throughout Catalonia (Fig. S1 in Supplementary material), and that were active during that period. The pollutants we were interested in for making spatial predictions were  $PM_{10}$ ,  $NO_2$ ,  $O_3$  and  $PM_{2.5}$  (all of them expressed as  $\mu m^3$ ) (air pollutants of interest, hereinafter). Nevertheless, the monitoring stations also measured other pollutants: nitrogen monoxide (NO), sulphur dioxide ( $SO_2$ ), carbon monoxide (CO), benzene ( $C_6H_6$ ), hydrogen sulphide ( $H_2S$ ), dichloride ( $Cl_2$ ), and heavy metals (mercury, arsenic, nickel, and lead). We have used these other pollutants as covariates.

Not all pollutants of interest were measured at all the monitoring stations. Thus, during the entire 2011–2020 period,  $PM_{10}$  was measured at 122 stations,  $NO_2$  at 77 stations,  $O_3$  at 62 stations and  $PM_{2.5}$  at 42 stations. As can be seen in Fig. 1, most of the monitoring stations were located in the city of Barcelona and in its metropolitan area. In the rest of the territory, the stations were located in cities (especially those that measure  $NO_2$  and  $PM_{2.5}$ ) and, in the case of  $O_3$ , also in rural areas. On the other hand, in 2020 (which we used to spatially predict short-term exposure), the number of air pollution monitoring stations dropped considerably; from 143 to 78. In particular, the number of stations measuring particles dropped dramatically (in the case of  $PM_{2.5}$  from 42 to 3, 92.88% fewer;  $PM_{10}$  from 122 to 36, 70.49% fewer). The number of stations measuring  $O_3$  went from 62 to 50 (19.35% fewer stations) and  $NO_2$  from 77 to 67 (12.99% fewer) (Table 1).

As our primary interest was in spatially predicting long-term exposure to air pollutants, we used the monthly averages, after obtaining the daily averages from the hourly data, from January 2011 to December 2019. To make the spatial predictions of the short-term exposure, we used the daily averages from January 1, 2020, to November 29, 2020.

We carried out the spatial predictions at a point level, with the centroids being Basic Health Areas (ABS, for its acronym in Catalan from here on). Catalan health planning defines an ABS as the elementary territorial unit through which primary health care services are organized (Atenció Primària Girona. Institut Català de la Salut, 2021). The ABSs are either made up of neighbourhoods or districts in urban areas, or by one or more municipalities in rural areas. Their delimitation is determined by geographical, demographic, social and epidemiological factors and, in particular, based on the accessibility the population has to services and the efficiency in the organization of health resources (Atenció Primària Girona, 2021). Catalonia is divided into 376 ABSs with populations between 371 and 72,321 inhabitants (mean 20,266 inhabitants, standard deviation 13,391, median 18,457 inhabitants, first quartile -Q1- 10,554, third quartile -Q3- 27,529). The population density was in the range of 0.31–34,590.58 inhabitants/ $km^2$  (mean 3,486.36, standard deviation 6,719.23, median 309.18, Q1 44.83, Q3 3,752.54). In Catalonia, 769 of the 947 of the municipalities belong to a single ABS. Of the 178 remaining, 46 were divided into more than one ABS, 37 of them into a maximum of five ABSs, eight between six and 14 ABSs and one, (the city of Barcelona) into 67 ABSs (Idescat, 2021).

Less than a third of the ABSs have at least one air pollution monitoring station (105 from a total of 376). That is, one ABS has five monitoring stations, six have three stations, 22 have two stations and the remaining 76 have only one station.

As covariates, we included the altitude of the air pollution monitoring station (in m) and the area of the ABS (in  $km^2$ ). The altitude (as well as other information related to the monitoring station, such as its latitude and longitude) were obtained from the Departament de Territori i Sostenibilitat (2021). We transformed the geographic coordinates (latitude and longitude) to UTM coordinates (in km) using the R package

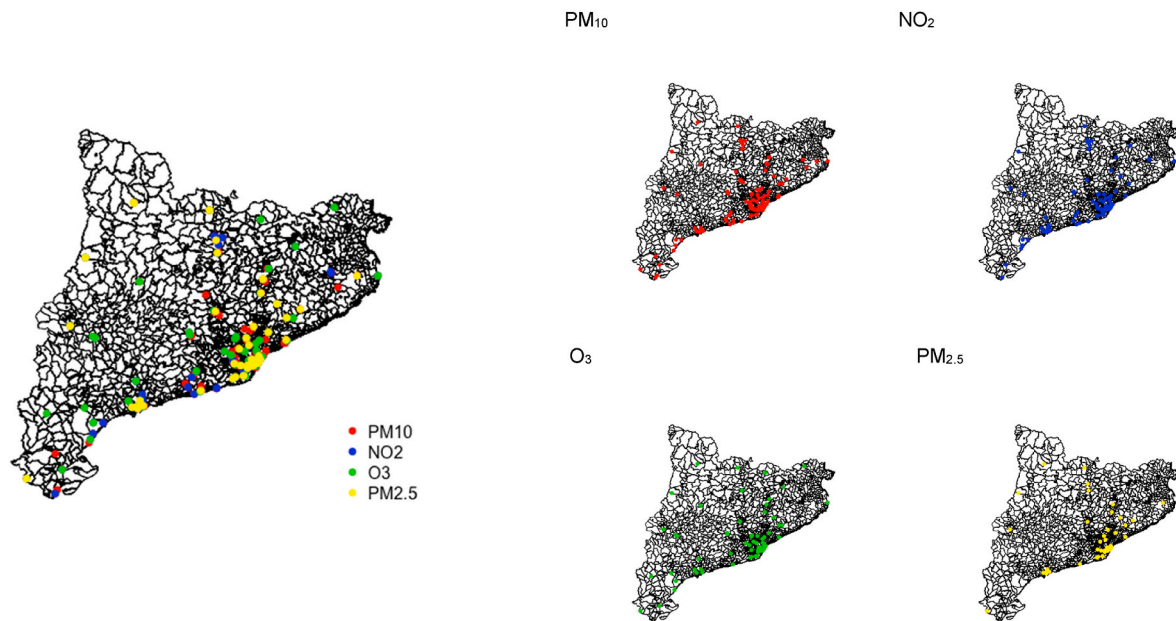


Fig. 1. Distribution in the territory of Catalonia (Spain), of the air pollution monitoring stations, according to where air pollutants (PM<sub>10</sub>, NO<sub>2</sub>, O<sub>3</sub> and PM<sub>2.5</sub>) are measured.

Table 1  
Description of the air pollutants.

	Long-term exposure			Short-term exposure			
	Number stations	2011–2018	2019	Number stations	Week 1–36, 2020	Week 1–10 and 26–36 (excluding lockdown), 2020	Week 37–48, 2020
<b>PM<sub>10</sub> (µm/m<sup>3</sup>)</b>	122			36			
mean (sd)		23.00 (7.79)	21.05 (6.37)		19.29 (9.85)	21.91 (10.96)	20.23 (11.34)
median [Q1-Q3]		22.32 [18.10–27.15]	20.68 [16.67–25.37]		17.83 [13.13–23.42]	20.29 [15.30–26.21]	18.08 [12.71–25.42]
<b>NO<sub>2</sub> (µm/m<sup>3</sup>)</b>	77			67			
mean (sd)		25.00 (15.10)	21.78 (12.76)		15.49 (12.04)	18.40 (13.36)	19.07 (12.98)
median [Q1-Q3]		23.59 [12.87–35.61]	20.92 [11.59–30.61]		12.25 [6.54–21.46]	15.21 [7.88–26.46]	17.11 [8.71–28.13]
<b>O<sub>3</sub> (µm/m<sup>3</sup>)</b>	62			50			
mean (sd)		53.64 (20.56)	55.77 (20.22)		55.23 (19.76)	50.90 (21.26)	44.55 (19.40)
median [Q1-Q3]		55.33 [37.62–68.86]	57.47 [39.60–70.15]		56.67 [43.92–68.00]	53.27 [36.58–64.79]	43.92 [30.25–58.42]
<b>PM<sub>2.5</sub> (µm/m<sup>3</sup>)</b>	42			3			
mean (sd)		13.98 (5.12)	10.85 (2.91)		11.42 (7.54)	11.94 (8.44)	10.30 (6.58)
median [Q1-Q3]		13.33 [10.47–16.75]	10.48 [9.86–11.57]		9.33 [5.86–14.51]	9.33 [5.66–15.34]	9.13 [5.45–14.02]
<b>Number of stations</b>	143			78			

Daily averages.

rgdal (Bivand et al., 2021). The areas of the ABS, as well as the UTM coordinates of their centroids, were calculated using QGIS (version 2.18) from the digitized cartography of the ABS (information of 2018) (open data) (Departament de Salut, 2021).

It is known that, at least in the short term, exposure to air pollution is correlated with various meteorological variables. For this reason, in the case of spatial prediction of short-term exposure, we also included several meteorological variables as covariates. Most of them, such as temperature (in °C), relative humidity (in %), wind speed at 10 m (in m/s) and atmospheric pressure (hPA), influence the dispersion of the pollutant; although some also influence its formation, for instance, global solar radiation (W/m<sup>2</sup>) (O<sub>3</sub> is a secondary pollutant, formed when the two atoms that make up oxygen gas dissociate under the action of light solar). The sources of the data were the stations in the Network of Automatic Meteorological Stations (XEMA) of the Meteorological

Service of Catalonia (METEOCAT) (open data). We also used the daily data from the State Meteorological Agency’s (AEMET) automatic stations.

The meteorological stations (albeit not as much as the air pollutant monitoring stations) are also dispersed throughout the territory. Catalonia has 217 meteorological stations: 188 belonging to METEOCAT and 29 to AEMET. All of them measured all the meteorological variables every day. In this case we had a spatial misalignment problem given that the meteorological station locations do not match the air pollutant monitoring locations. To address this problem, and along the lines of Wright et al. (2021), we jointly model air pollutants and meteorological variables. Further details can be found in Barceló et al. (2016).

## 2.2. Model specification

We specified a hierarchical spatiotemporal model as follows:

At the top of the hierarchy:

$$Z(s_i, t) = Y(s_i, t) + \varepsilon(s_i, t) \quad [1]$$

where  $i$  denoted the air pollution monitoring station where the pollutant was observed;  $t$  was the time unit;  $s_i$  the location of the station;  $Y(\cdot, \cdot)$  the spatiotemporal process, the realization of which corresponded to the pollutant measurements (at station  $i$  and time unit  $t$ ); and  $\varepsilon(\cdot, \cdot)$  the measurement error defined by a Gaussian white-noise process (i.e., spatially and temporally uncorrelated) (the variance of the measurement error,  $\sigma_\varepsilon^2$ , was the nugget effect).

The spatiotemporal process,  $Y(\cdot, \cdot)$  was an independent in time Gaussian field (GF) with zero mean and a Matérn covariance function:

$$\text{Cov}(\eta(s_i, t), \eta(s'_i, t)) = \frac{\sigma^2}{2^{\nu-1}\Gamma(\nu)} (\kappa s_i - s'_i)^\nu K_\nu(\kappa |s_i - s'_i|) \quad [2]$$

Where  $\eta(\cdot, \cdot)$  denotes a spatiotemporal process.  $K_\nu$  is the modified Bessel function of the second type and order  $\nu > 0$ .  $\nu$  is a parameter controlling the smoothness of the GF,  $\sigma^2$  is the variance and  $\kappa > 0$ , is a scaling parameter related to the range,  $\rho$ , the distance to which the spatial correlation becomes small. We used  $\rho = \sqrt{8\nu}/\kappa$ , where  $\rho$  corresponded to the distance where the spatial correlation is close to 0.1 for each  $\nu$  (Lindgren et al., 2011).  $\kappa = 2\varphi\sqrt{\nu}$ , where  $\varphi$  is a parameter controlling the rate of decay of the spatial correlation as the distance  $s_i - s'_i$  increases.

At the next level, we specified the following measurement equation:

$$y(s_i, t) = \mu(s_i, t) + \eta(s_i, t) \quad [3]$$

where  $y(\cdot, \cdot)$ , is the realization of the spatiotemporal process  $Y(\cdot, \cdot)$ ;  $\mu(\cdot, \cdot)$  denoted the large-scale component, depending on the covariates; and  $\eta(\cdot, \cdot)$  was a spatiotemporal process.

Due to its computational problems, we chose to represent the GF as a Gaussian Markov Random Field (GMRF) (Rue et al., 2009). GMRFs are defined by a precision matrix with a sparse structure allowing inference to be performed in a computationally effective way. We linked the GF and GMRF through the Stochastic Partial Differential Equations (SPDE) approach (Lindgren et al., 2011). The SPDE allowed us to find a GMRF, with local neighbourhood and sparse precision matrix (instead of spatiotemporal covariance function and the dense covariance matrix of a GF, respectively), that best represented the Matérn field. Further details can be found in Lindgren et al. (2011) and in Cameletti et al. (2013).

We specified the large-scale component,  $\mu(\cdot, \cdot)$ , as a generalized linear mixed model (GLMM) with response from the Gaussian family. Specifically, for each of the pollutants of interest (PM<sub>10</sub>, NO<sub>2</sub>, O<sub>3</sub> and PM<sub>2.5</sub>) we specified two GLMMs: one for long-term exposure and the other for short-term exposure.

Long-term exposure:

$$\mu_{i,t} = \beta_0 + \sum_{j=1}^{14} \beta_j \text{pollutant}_{j,it} + \beta_{15} \text{altitude}_i + \beta_{16} \text{area}_i + sd\_y_{i,\text{year}} + \omega_i + \tau_{\text{month}}$$

Short-term exposure:

$$\begin{aligned} \mu_{i,t} = & \beta_0 + \sum_{j=1}^{14} \beta_j \text{pollutant}_{j,it} + \beta_{15} \text{temperature}_{it} + \beta_{16} \text{relative humidity}_{it} + \beta_{17} \text{wind speed}_{it} + \beta_{18} \text{atmospheric pressure}_{it} + \beta_{19} \text{solar radiation}_{it} + \beta_{20} \text{altitude}_i \\ & + \beta_{21} \text{area}_i + sd\_y_{i,\text{week}} + \omega_i + \tau_{\text{day}} \end{aligned}$$

where  $i$  denoted the air pollution monitoring station where the pollutant was observed ( $i = 1, 2, \dots, 143$ );  $t$  was the time unit (month in the case of long-term exposure, day in the case of short-term exposure);  $\mu_{i,t} = E(y_{i,t})$ ,  $y_{i,t}$  denoted the air pollutants of interest, PM<sub>10</sub>, NO<sub>2</sub>, O<sub>3</sub> and PM<sub>2.5</sub>;  $\text{pollutant}_{j,it}$  corresponded to the pollutant  $j$  measurements at station  $i$  and time unit  $t$ . Pollutants considered were, first, the pollutants of interest other than the pollutant for which the spatial prediction was made and, second, the rest of the pollutants (i.e., NO, SO<sub>2</sub>, CO, C<sub>6</sub>H<sub>6</sub>, H<sub>2</sub>S, Cl<sub>2</sub>, mercury, arsenic, nickel, and lead);  $\text{area}_i$  was the area of the ABS  $i$ ;  $sd\_y_{i,\cdot}$ ,  $\eta_i$  and  $\tau$  denoted random effects.

In the models, we included  $sd\_y_{i,\text{year}}$ ,  $sd\_y_{i,\text{week}}$  structured random effects, indexed on a standard deviation of the air pollutant that was being predicted, in the ABS  $i$ , during a particular year (2011–2018) and a particular week of 2020 (weeks 1–37), respectively. We chose a random walk of order one (rw1) as the structure of the random effect. In the integrated nested Laplace approximations (INLA) approach (Rue et al., 2009, 2017), the random walk of order 1 for the Gaussian vector  $x$  is constructed assuming independent increments (R INLA project, 2021a):

$$\Delta x_i = x_i - x_{i-1} \sim N(0, \sigma_x^2)$$

Following the INLA approach when, as in our case, the random effects are indexed on a continuous variable (such as  $sd\_y_{i,\text{year}}$ ,  $sd\_y_{i,\text{week}}$ ,  $\tau_{\text{month}}$  and  $\tau_{\text{day}}$ ), they can be used as smoothers to model non-linear dependency on covariates in the linear predictor.

$\omega_i$  denoted a random effect indexed on the air pollution monitoring station. This random effect was unstructured (independent and identically distributed random effects) and captured individual heterogeneity, i.e., unobserved confounders specific to the station and invariant in time.

We also included  $\tau_{\text{month}}$  and  $\tau_{\text{day}}$ , structured random effects indexed on time, in order to control the temporal dependency associated to possible seasonal effects throughout the year (long-term exposure) and throughout the week (short-term exposure). In this case, a model for seasonal variation with periodicity  $m$  (12 for long-term exposure, seven for short-term exposure), for the random vector  $(x_1, x_2, \dots, x_n)$  ( $n > m$ ) was obtained assuming that the sums were independent Gaussian with a precision  $\tau$ . The density for  $x$  is derived from the  $n-m+1$  increments (R INLA project, 2021b):

$$\frac{\tau^{\frac{n-m+1}{2}}}{e^{-\frac{\tau}{2} \sum (x_i + x_{i+1} + \dots + x_{i+m-1})^2}}$$

## 2.3. Inference

Inferences for GMRFs were made following a Bayesian perspective using the INLA approach (Rue et al., 2009, 2017).

We started from the SPDE representation, which uses a finite element representation to define the Matérn field as a linear combination of basis functions defined on a triangulation of the domain (mesh, hereinafter). This consists of subdividing the domain into a set of non-intersecting triangles meeting in, at most, a common edge or corner (Lindgren et al., 2011; Cameletti et al., 2013).

Then, instead of projecting the subsequent mean of the random field onto mesh nodes to target locations where we do not have observed

data, we performed the spatial prediction of the random field jointly with the parameter estimation process. For this, we projected the mesh into those locations with no air pollutants observed and then we jointly computed the posterior means at all the locations (with observed and unobserved air pollutants measurements) (Krainski et al., 2020).

We separately estimated each year (long-term exposure) and each week (short-term exposure) and then merged every year and every week.

We used priors that penalize complexity (PC priors). These priors are robust in that they do not have an impact on the results and, furthermore, they have an epidemiological interpretation (Simpson et al., 2017).

All analyses were carried out using the free software R (version 4.0.3), through the INLA package (Rue et al., 2009, 2017; R INLA project, 2021c). The maps were represented using the leaflet package (Cheng et al., 2019).

### 2.4. Measures of predictive performance

The predictive performance of each model was assessed by cross-validation, considering a training set (2011–2018 for long-term exposure, weeks 1–36 - January 1 to September 8, 2020 -, for short-term

$$\mu_{i,t} = \beta_0 + \sum_{j=1}^{14} \beta_j \text{pollutant}_{j,i,t} + \beta_{15} \text{altitude}_i + \beta_{16} \text{area}_i + \text{sd}_{-y_i, \text{year}} + \eta_i + \tau_{\text{month}} + \tau_{\text{year}}$$

exposure) and a test set (2019 for long-term exposure and weeks 37 - September 9 - to 48 - November 29, 2020-for short-term exposure).

The prediction accuracy was assessed by:

- Mean absolute percentage error (MAPE)

$$\text{MAPE} = \frac{1}{N} \sum_i \sum_t \left| \frac{y(s_i, t) - \hat{y}(s_i, t)}{\hat{y}(s_i, t)} \right| * 100$$

where N was the total number of available observations in the test set;  $y(s_i, t)$  were the pollutant measurements (at station i and time unit t) at the test set; and  $\hat{y}(s_i, t)$  were the posterior means.

- Root mean square error (RMSE)

$$\text{RMSE} = \sqrt{\frac{1}{N} \sum_i \sum_t (y(s_i, t) - \hat{y}(s_i, t))^2}$$

- Correlation coefficient

$$r = \frac{\sum_i \sum_t (y(s_i, t) - \overline{y(s_i, t)}) (\hat{y}(s_i, t) - \overline{\hat{y}(s_i, t)})}{(\sum_i \sum_t (y(s_i, t) - \overline{y(s_i, t)})^2 \sum_i \sum_t (\hat{y}(s_i, t) - \overline{\hat{y}(s_i, t)})^2)^{\frac{1}{2}}}$$

- Actual coverage of the 95% prediction intervals

### 2.5. Sensitivity analysis

We conducted two sensitivity analyses. First, we carried out a new cross-validation and then we changed the spatiotemporal model. In both cases, we consider the spatial prediction of long-term exposure to NO<sub>2</sub>.

As regards cross-validation, we considered five random samples from the monitoring stations in which NO<sub>2</sub> was measured during the entire period 2011–2019 as training sets. Specifically, we considered random samples of approximately 75% of the stations (58 out of a total of 77 stations), of 70% (55 stations), 50% (41 stations), 45% (35 stations), and

20% (18 stations). As a test set, we considered the rest of the stations (19, 22, 36, 42 and 59 remaining stations, respectively).

Next, we calculated the measures' prediction accuracy (explained previously).

With respect to the spatiotemporal model above, we considered an independent in time Gaussian field (GF), and following Camellei et al. (2013) we assumed a spatiotemporal Gaussian field that changes in time according to an autoregressive of order one (AR(1)).

Returning the measurement equation {2}:

$$y(s_i, t) = \mu(s_i, t) + \eta(s_i, t) \tag{2a}$$

the realization of the spatiotemporal process,  $\eta(\cdot, \cdot)$ , was specified as,

$$\eta(s_i, t) = \varphi \eta(s_i, t - 1) + \omega(s_i, t) \tag{4}$$

where  $|\varphi| < 1$ .

Here, it was  $\omega(s_i, t)$  which was assumed to be a zero mean Gaussian and a Matérn covariance function (equation {3}).

In the addition, in the GLMM specification of the large-scale component,  $\mu(\cdot, \cdot)$ , in the linear predictor we included structured random effects indexed on year,  $\tau_{\text{year}}$ , to capture the long-term trend.

With this analysis, our objective was to compare not only the predictive performance of the model {1–2}, {4–5} with the one specified above {1–3} but, above all, to compare the computation time in the inference of both specifications.

### 3. Results

Descriptive results are shown in Table 1. Regarding long-term exposure, we observed that, apart from O<sub>3</sub>, the daily averages of pollutants decreased in 2019 (PM<sub>2.5</sub> 22.39% less, NO<sub>2</sub> 12.88% less and PM<sub>10</sub> 8.48% less). In contrast, the daily average of O<sub>3</sub> increased by 3.97% in 2019 compared to 2011–2018. With regard to short-term exposure, the levels of NO<sub>2</sub> and PM<sub>10</sub> were higher from September 9 (week 37) (23.11% and 4.87%, respectively). Conversely, the levels of O<sub>3</sub> and PM<sub>2.5</sub> (although in this case only measured in three stations) were lower than the levels before September 9 (19.34% and 9.81%). When we excluded the lockdown (in Spain this took place from March

**Table 2**  
Description of the spatial predictions of air pollutants.

PM <sub>10</sub> (µm/m <sup>3</sup> )	
mean (sd)	21.33 (5.59)
median [Q1-Q3]	20.78 [17.10–25.04]
minimum, maximum	9.71, 35.58
NO <sub>2</sub> (µm/m <sup>3</sup> )	
mean (sd)	25.92 (11.41)
median [Q1-Q3]	23.37 [16.80–34.73]
minimum, maximum	4.33, 58.14
O <sub>3</sub> (µm/m <sup>3</sup> )	
mean (sd)	53.91 (16.96)
median [Q1-Q3]	54.93 [42.02–70.08]
minimum, maximum	10.37, 80.02
PM <sub>2.5</sub> (µm/m <sup>3</sup> )	
mean (sd)	7.53 (5.69)
median [Q1-Q3]	8.52 [1.62–11.91]
minimum-maximum	0.31, 25.28

**Table 3**  
Measures of predictive performance. Spatiotemporal process independent in time Gaussian field.

Long-term exposure				
	MAPE	RMSE	Correlation	Coverage
PM <sub>10</sub>	7.429%	2.640	0.838	0.917
NO <sub>2</sub>	4.345%	2.930	0.937	0.973
O <sub>3</sub>	6.795%	5.287	0.916	0.945
PM <sub>2.5</sub>	16.037%	3.068	0.696	0.750
Short-term exposure – Training set Weeks 1–37				
	MAPE	RMSE	Correlation	Coverage
PM <sub>10</sub>	15.263%	6.002	0.401	0.441
NO <sub>2</sub>	17.119%	7.920	0.801	0.840
O <sub>3</sub>	19.323%	9.530	0.832	0.835
PM <sub>2.5</sub>	45.169%	6.103	0.400	0.078
Short-term exposure – Training set Weeks 1–10 and 26–36 (excluding lockdown)				
	MAPE	RMSE	Correlation	Coverage
PM <sub>10</sub>	14.002%	5.910	0.469	0.497
NO <sub>2</sub>	7.122%	5.623	0.901	0.910
O <sub>3</sub>	9.023%	7.002	0.865	0.899
PM <sub>2.5</sub>	38.532%	5.489	0.402	0.083

MAPE: Mean absolute percentage error.  
 RMSE: Root mean square error.  
 Correlation: Correlation coefficient.  
 Coverage: Actual coverage of the 95% prediction credibility intervals.

14 - week 11- to June 21 - week 25 -, both 2020), the variations from September 9 changed sign for PM<sub>10</sub>, it was 7.67% lower, they were moderated for NO<sub>2</sub> (which was 3.64% higher) and O<sub>3</sub> (12.48% lower), while they were increased in the case of PM<sub>2.5</sub> (13.74% lower).

In the Supplementary material we provide some results of fitting the models for long-term exposure. In Table S1 we show the results for the hyperparameters of the model, as well as various measures of goodness-of-fit and complexity of the model. In Fig. S2, the posterior distribution of the betas of the fixed effects and in Fig. S3, the posterior means of the fitted values of the long-term exposure to air pollutants by ABS vs. the observed levels of the air pollutants in each ABS. As can be seen, the fit was quite good in all cases.

In Table 2 we show some descriptions of the spatial predictions. In particular, we would like to point out the symmetry of the predictions (means and medians are similar in all cases) and the non-existence of negative values in the predictions.

The measures of predictive performance are shown in Table 3. Except for PM<sub>2.5</sub>, the results for long-term exposure were quite good. Achieved coverages of the 95% credibility intervals for predictions were greater than 90%, correlation coefficients were greater than 0.80, and MAPEs less than 10%. Furthermore, if Table 3 is compared with Table 1, it is observed that the reduction in the variability of the spatial prediction, measured between the ratio of the RMSE and the standard deviations of the pollutants observed, was, at most, one third of the standard deviations of the pollutants during the period 2011–2018 (19.40% for NO<sub>2</sub>, 25.71% for O<sub>3</sub> and 33.89% for PM<sub>10</sub>), again with the exception of PM<sub>2.5</sub> (the RMSE in this case was 59.92% of the standard deviation in the period 2011–2018). Therefore, except for PM<sub>2.5</sub>, our method managed to significantly reduce the variability of the spatial prediction around fairly accurate predictions. Although quite good note that, in relative terms, the results for PM<sub>10</sub> were somewhat worse than for gaseous pollutants (NO<sub>2</sub> and O<sub>3</sub>).

The poor results obtained for PM<sub>2.5</sub> are because of its smaller sample size. Although it is true that in the period as a whole up to 42 stations measured PM<sub>2.5</sub>, the year with the lowest number of active stations was 2018 (31 stations), with the rest of the years ranging between 33 and 35 active stations. No year fell below 40 active stations for the rest of pollutants (the year with the lowest number of stations measuring PM<sub>10</sub> was 2018 with 94 stations, while the other years ranged between 100 and 107 stations; in the cases of NO<sub>2</sub> and O<sub>3</sub> it was 2015 with 59 and 44

**Table 4**  
Sensitivity analyses. Measures of predictive performance.

NO <sub>2</sub> , Long-term exposure 2011–2019.				
Total of active monitoring stations in the period: 77				
Spatiotemporal process independent in time Gaussian field				
	MAPE	RMSE	Correlation	Coverage
Training set 58 monitoring stations (75%)	4.973%	3.205	0.930	0.963
Training set 55 monitoring stations (70%)	5.902%	6.464	0.851	0.925
Training set 41 monitoring stations (50%)	6.072%	7.201	0.786	0.870
Training set 35 monitoring stations (45%)	8.020%	8.088	0.776	0.633
Training set 18 monitoring stations (20%)	8.806%	10.159	0.609	0.590
Spatiotemporal Gaussian field that changed in time according to an autoregressive of order one (AR(1))				
Long-term exposure				
	MAPE	RMSE	Correlation	Coverage
NO <sub>2</sub>	8.843%	3.388	0.957	0.958

MAPE: Mean absolute percentage error.  
 RMSE: Root mean square error.  
 Correlation: Correlation coefficient.  
 Coverage: Actual coverage of the 95% prediction credibility intervals.

stations, respectively, with the other years oscillating between 62 and 66, and 45 and 57, respectively).

Regarding the short-term exposure, first, the predictive performance was worse when we did not exclude the lockdown period (which took place in Spain from March 14 to June 21, 2020) than when we did. In fact, note that the predictive performance measures were much better for gaseous pollutants (NO<sub>2</sub> and O<sub>3</sub>). The results for the coarse particles, PM<sub>10</sub>, were quite poor (we did not interpret the results for PM<sub>2.5</sub> as it was measured in only three stations). This was likely due to the lower number of stations where PM<sub>10</sub> was measured (36 stations, versus 67 for NO<sub>2</sub> and 50 for O<sub>3</sub>, see Table 1). The variability of the spatial prediction was reduced by much less than in long-term exposure, especially for NO<sub>2</sub>. The RMSEs were between 36.09% for O<sub>3</sub> and 54.86% for NO<sub>2</sub>, of the standard deviations of the pollutants (excluding lockdown).

The results of the sensitivity analyses, when the number of stations in the training set was greater than 40 and when the spatiotemporal Gaussian field changed in time according to an AR(1) (model {1–2}, {4–5}), were quite similar to the results for the spatiotemporal process independent in time Gaussian field (model {1–3}) and all the stations were included in the training set (Table 4).

When we varied the number of stations in the training set but used every year (2011–2019), the predictive performance seemed to depend on the size of the sample. The more stations the training set had, the better the results were. In other words, dramatically deteriorating with a small sample size. In fact, the cut-off appears to be 40 stations. Below this, the predictive performance measures were poor.

Although the predictive performance of the spatiotemporal Gaussian field model changed in time according to an AR (1), (model {1–2}, {4–5}) was very similar to that of the spatiotemporal process independent in time Gaussian field (model {1–3}) (perhaps somewhat worse, in relative terms), the computation time was much longer. Using a 6-core Intel Core i9 (2.9 GHz 32 GB RAM), while the model inference {1–3} required on average 0.05 s per observation (a total of 569 s on average), the model {1–2}, {4–5} required 0.354 s (a total of 3,947 s), that is, seven times more computing time.

The maps of the posterior means and the posterior standard deviations for 2019 (in quintiles) of the spatiotemporal process independent in time Gaussian field (model {1–3}) for the long-term exposure of PM<sub>10</sub>, NO<sub>2</sub> and O<sub>3</sub> are shown in Fig. 2. We decided not to represent the

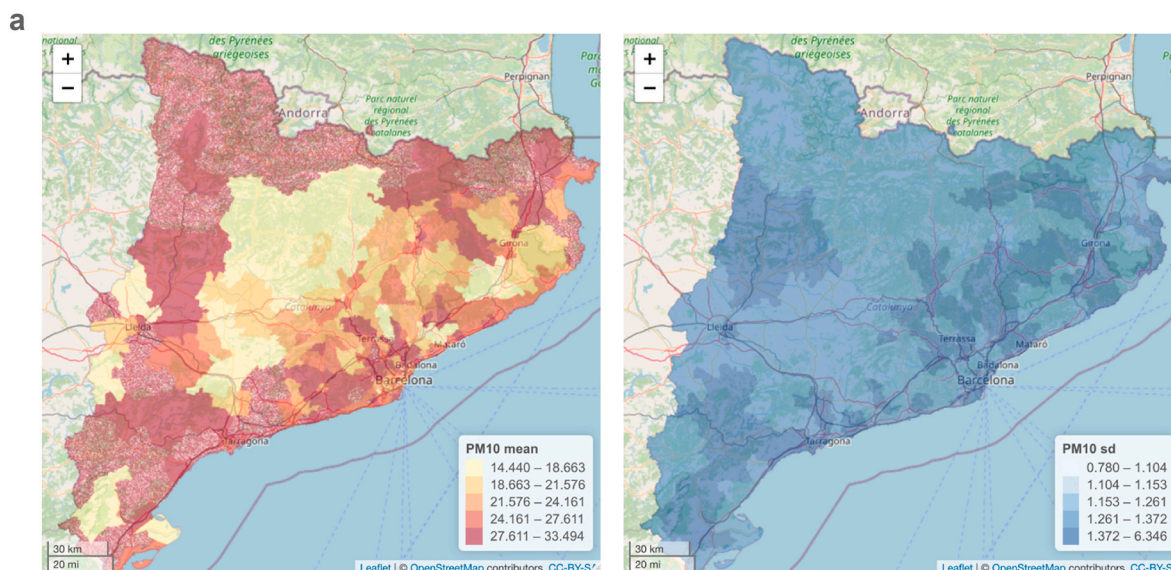


Fig. 2a. Posterior mean and posterior standard deviation of PM10 for 2019. Spatiotemporal process independent in time Gaussian field.

posterior means for PM<sub>2.5</sub> because of its poor predictive performance. The spatial distributions of the subsequent means of PM<sub>10</sub> and NO<sub>2</sub> were quite similar, although in the high levels of NO<sub>2</sub>, (fourth and fifth quintiles) there was somewhat more spatial variation. Note that, unlike PM<sub>10</sub> and NO<sub>2</sub>, the lowest levels of O<sub>3</sub> (first and second quintiles) occurred in the urban areas. As expected, the uncertainty, as measured by the posterior standard deviations, was, in general, higher in those areas with few (or no) monitoring stations. Note, however, that higher levels of air pollutants do not always coincide with higher standard deviations.

#### 4. Discussion

Our results were quite good in terms of predictive performance, at least for those pollutants that were observed in more than 40 collecting stations (PM<sub>10</sub>, NO<sub>2</sub> and O<sub>3</sub> in long-term exposure and NO<sub>2</sub> and O<sub>3</sub> in short-term exposure).

The current coverage of the spatial predictions of these pollutants are in line with similar studies. Using the same model and the same data (PM<sub>10</sub>), but applying two different methods for the inference, Cameletti et al. find coverage between 0.95 and 0.97 (using MCMC) (Cameletti et al., 2011) and 0.897 (using INLA SPDE) (Cameletti et al., 2013). Mukhopadhyay and Sahu (2018) find coverage between 0.91 and 0.92 for the spatial predictions for O<sub>3</sub> (in our case, 0.89 for short-term exposure and 0.945 for long-term exposure), between 0.89 and 0.90 for PM<sub>10</sub> (in our case, 0.917 for long-term exposure) and between 0.95 and 0.965 for NO<sub>2</sub> (in our case, 0.905 for short-term exposure and 0.963 for long-term exposure). Note: we have preferred not to comment on the results in which we found poor predictive performance. Our coverage could also be comparable to those provided by Pirani et al. (2013) for the spatial predictions for PM<sub>10</sub> (between 0.87 and 0.93), although it should be noted that these show the coverage at 90%.

The correlation coefficients between the observed levels of air pollutants and the subsequent means of the spatial predictions are in the range reported in Fiovaranti et al. (2021) for PM<sub>10</sub> (0.79–0.91). In our case, they were higher than in Cameletti et al. (0.863 when the inferences were made with MCMC - Cameletti et al., 2011- and 0.702 when they were made with INLA SPDE - Cameletti et al., 2013-, compared to 0.917 in our case), or than in Pirani et al. (2013) (between 0.73 and 0.78), in both cases for PM<sub>10</sub>. However, they were somewhat lower than in Mukhopadhyay and Sahu (2018) (0.88–0.89 for PM<sub>10</sub>, 0.92–0.94 for NO<sub>2</sub>, and 0.93–0.94 for O<sub>3</sub>). It should be said, nonetheless,

that the number of observations in Mukhopadhyay and Sahu range between 56,625 (for PM<sub>10</sub>) and 100,138 (for NO<sub>2</sub>), while in our case we had 11,157 observations.

The reduction in the variability of the spatial prediction can only be compared with Mukhopadhyay and Sahu (2018), since they are the only ones who show these standard deviations. In this sense, both Mukhopadhyay and Sahu and ourselves achieved a similar reduction in the variability of the spatial prediction.

Although good, the results of the predictive performance were less so for the spatial prediction of long-term exposure to PM<sub>10</sub> (despite being observed in the largest number of collecting stations, see Table 1) and for the short-term exposure for gaseous pollutants (NO<sub>2</sub> and O<sub>3</sub>).

Regarding the spatial prediction of long-term exposure to PM<sub>10</sub>, we believe that it is a consequence of the location of the monitoring stations. The stations that measure PM<sub>10</sub>, although more abundant in urban areas, are also located in rural areas, while those that measure NO<sub>2</sub> are located almost exclusively in urban areas. In the city of Barcelona, even though 13% of NO<sub>2</sub> is generated outside the municipality, it is 71% in the case of PM<sub>10</sub> (Barcelona City Council, 2015; Saez et al., 2020). It is not unreasonable to suppose that these figures can be extrapolated to the entire Barcelona Metropolitan Area, which comprises 41.75% of the total population of Catalonia and where the majority of PM<sub>10</sub> and NO<sub>2</sub> monitoring stations are located. In other words, while NO<sub>2</sub> monitoring stations measured almost all the NO<sub>2</sub> pollution, PM<sub>10</sub> monitoring stations did not collect all the PM<sub>10</sub> pollution data. This could also explain why the posterior means of the PM<sub>10</sub> predictions exhibited less spatial variability than the NO<sub>2</sub> predictions (Fig. 2a and b).

With regard to the spatial predictions of short-term exposure, the reduction in the number of monitoring stations during 2020 could have led to a deterioration in the predictive performance. However, we believe it could also be due to the data behaviour during 2020. As a consequence of the lockdown to flatten the COVID-19 pandemic curve, mobility was greatly reduced in 2020. Specifically, mobility was reduced by 40% on average, compared to pre-COVID-19 levels, during the lockdown and did not fully recover in the September–November 2020 period (being 5–15% lower, depending on the area of Catalonia [26]). We are sure that this anomalous behaviour would have influenced the predictive performance of the spatial predictions of short-term exposure.

The predictive performance of our model depends on the number of stations where pollutants are measured. We have found that with fewer than 40 stations, probably spread throughout the territory (although not

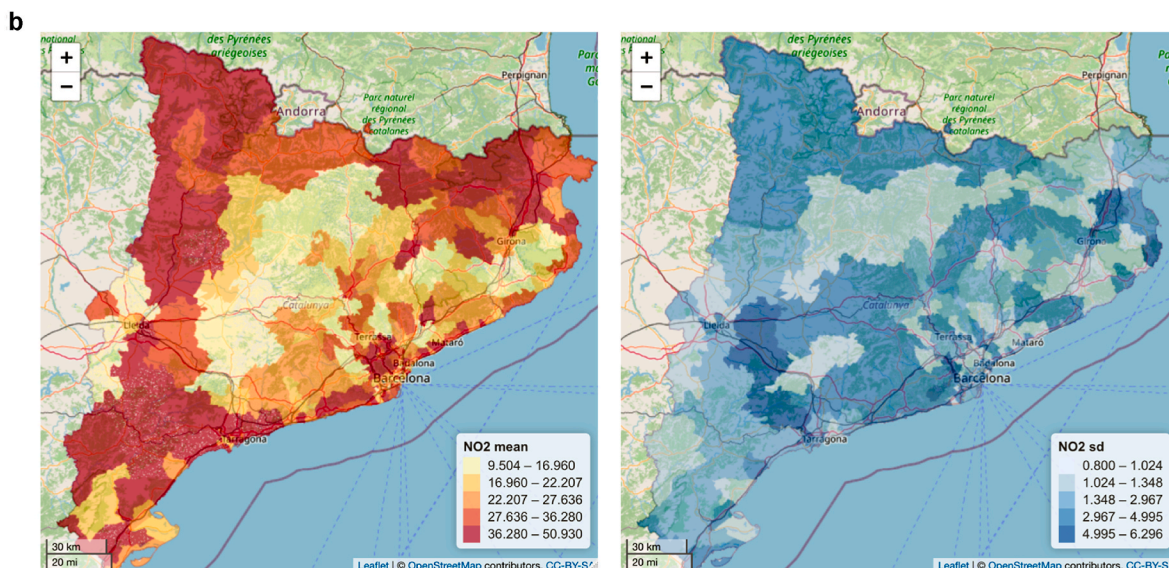


Fig. 2b. Posterior mean and posterior standard deviation of NO2 for 2019. Spatiotemporal process independent in time Gaussian field.

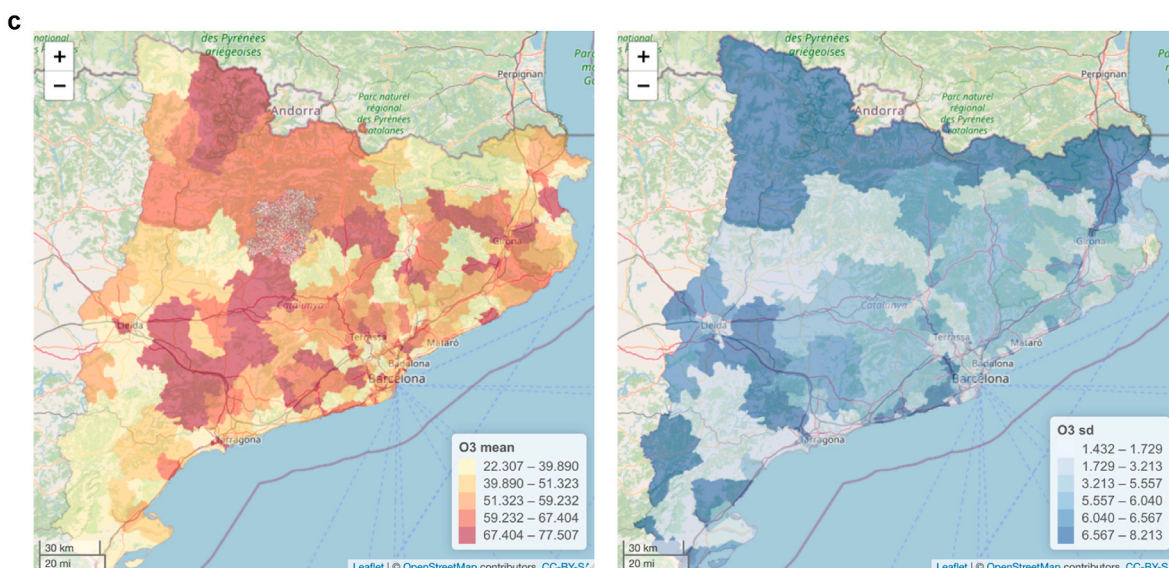


Fig. 2c. Posterior mean and posterior standard deviation of O3 for 2019. Spatiotemporal process independent in time Gaussian field.

necessarily homogeneously), the predictive performance deteriorates considerably.

Our method is quite similar to that of [Camelleti et al. \(2013\)](#). However, as we show with the sensitivity analysis, our method, in which we perform the inference year by year (or week by week) and then merge the subsequent ones, has a much shorter computation time, in addition to somewhat better results, even for such an atypical year such as 2020.

In our study we preferred to use a hierarchical Bayesian model rather than, for example, atmospheric chemistry models. There reasons why we chose our approach are two-fold. First, and most importantly, we are interested in predicting at a higher spatio-temporal resolution than is usually handled by atmospheric chemistry models (up to one hundredth of a degree by one hundredth of a degree) and, second, these models do not usually take into account temporal and spatial dependencies, which hierarchical Bayesian models do.

We believe that several points warrant further investigation. First, we are convinced that our results might not be as good if the spatial and temporal dimensions were dependent and not separable, that is, if the spatial dependence varied over time. Fortunately, the spatial

dependence of air pollutants does not vary over time. Even during 2020, although air pollution levels decreased as a consequence of the reduction in mobility, the spatial dependence was more or less similar to previous years. For spatial dependence to vary over time, major changes in infrastructures or, likewise, lasting limitations in mobility that were not homogeneous throughout the territory be produced. Of course, other types of spatiotemporal data could imply other results. Spatial prediction when spatial and temporal dependencies are non-separable requires other more complex methods, in line with [Krainski's non-separable space-time models \(2018\)](#), which are a derivation of the iterated heat equation with spatially correlated driving noise.

Second, air pollution exposure misclassification due to between-area mobility and within-area variation should be mitigated using, for example, the methods proposed by [Richmond-Bryant and Long \(2020\)](#) to help mitigate the impact of measurement error.

Another problem that deserves further investigation is non-stationarity in variance. For this we will start from the works of [Ossandón et al. \(2021\)](#) and [Verdin et al. \(2019\)](#), who model the spatial process by adjusting a hierarchical model at each location and apply a

spatial process on the betas. This enables us to also model the variance spatially.

## 5. Conclusion

In this work, we have shown a hierarchical Bayesian spatiotemporal model that has allowed us to make fairly accurate spatial predictions with a low computational cost. Our model provides predictions of both long-term and short-term exposure. The only requirements of the method that we propose lie in a minimum number of stations being distributed throughout the territory where the prediction is to be made and that the spatial and temporal dimensions are either independent or separable.

## Software and data availability

We used open data with free access from these sources.

### Air pollutants

Departament de Territori i Sostenibilitat, Generalitat de Catalunya [Available at: <https://analisi.transparenciacatalunya.cat/en/Medi-Ambient/Qualitat-de-l-aire-als-punts-de-mesurament-autom-t/tasf-thgu>, last accessed on March 14, 2021].

### Meteorological variables

METEOCAT, Generalitat de Catalunya. Meteorological data from XEMA [Available at: <https://analisi.transparenciacatalunya.cat/en/Medi-Ambient/Dades-meteorol-giques-de-la-XEMA/nzvn-apee>, last accessed on March 14, 2021].

AEMET. AEMET Open Data [in Spanish] [Available at: [http://www.aemet.es/es/datos\\_abiertos/AEMET\\_OpenData](http://www.aemet.es/es/datos_abiertos/AEMET_OpenData), last accessed on March 14, 2021].

### Digitized cartography of the ABS

Departament de Salut. Cartography [Available at: [https://salutweb.gencat.cat/ca/el\\_departament/estadistiques\\_sanitaries/cartografia/](https://salutweb.gencat.cat/ca/el_departament/estadistiques_sanitaries/cartografia/), accessed on March 14, 2021].

Code will be available at [www.researchprojects.es](http://www.researchprojects.es).

## Authorship

MS had the original idea for the paper and designed the study. The bibliographic search and the writing of the introduction were carried out by MS and MAB. The methods and statistical analysis were chosen and performed by MS. MAB created the tables and figures. MS and MAB wrote the results and the discussion. The writing and final editing was done by all authors. MS and MAB reviewed and approved the manuscript.

## Funding

This work was partially financed by the SUPERA COVID19 Fund, from SAUN: Santander Universidades, CRUE and CSIC, and by the COVID-19 Competitive Grant Program from Pfizer Global Medical Grants. It also received funding, in the form of a free transfer of data, from AEMET. The funding sources did not participate in the design or conduct of the study, the collection, management, analysis or interpretation of the data, or the preparation, review or approval of the manuscript.

## Ethics

Not applicable.

## Declaration of competing interest

The authors declare that they have no known competing financial interests or personal relationships that could have appeared to influence the work reported in this paper.

## Acknowledgements

This study was carried out within the ‘Cohort-Real World Data’ subprogram of CIBER of Epidemiology and Public Health (CIBERESP). We appreciate the comments of three anonymous reviewers of a previous version of this work who, without doubt, helped us to improve our work. The usual disclaimer applies.

## Appendix A. Supplementary data

Supplementary data to this article can be found online at <https://doi.org/10.1016/j.envsoft.2022.105369>.

## References

- AEMET. AEMET Open Data [in Spanish] [Available at: [http://www.aemet.es/datos\\_abiertos/AEMET\\_OpenData](http://www.aemet.es/datos_abiertos/AEMET_OpenData). (Accessed 27 February 2021). last accessed on.
- Atenció Primària Girona. Institut Català de la Salut. Basic Health Areas (ABS) [in Catalan] [Available at: <http://www.icsgirona.cat/ca/contingut/primaria/370>. (Accessed 27 February 2021). last accessed on.
- Bakar, K.S., Sahu, S.K., 2015. spTimer: spatio-temporal Bayesian modelling using R. *J. Stat. Software* 63 (15), 1–32. <https://doi.org/10.18637/jss.v063.i15>.
- Barceló, M.A., Varga, D., Tobias, A., Díaz, J., Linares, C., Saez, M., 2016. Long term effects of traffic noise on mortality in the city of Barcelona. *Environ. Res.* 147, 193–206. <https://doi.org/10.1016/j.envres.2016.02.010>, 2004–2007.
- Barcelona City Council, 2015–2018. Barcelona air quality improvement plan [in Catalan] [Available at: last accessed on March 14, 2021]. <https://ajuntament.barcelona.cat/ecologiaurbana/ca/que-fem-i-per-que/ciutat-productiva-i-resilient/pla-de-qualitat-de-l-aire-de-bcn>.
- Bivand, R., Keitt, T., Rowlingson, B. rgdal: Bindings for the ‘Geospatial’ Data Abstraction Library. R package version 1.5-8 [Available at: <https://CRAN.R-project.org/package=rgdal>. (Accessed 27 February 2021). last accessed on.
- Calculi, C., Fassò, A., Finazzi, F., Pollice, A., Turnone, A., 2015. Maximum likelihood estimation of the multivariate hidden dynamic geostatistical model with application to air quality in Apulia, Italy. *Environmetrics* 26 (6), 406–417. <https://doi.org/10.1002/env.2345>.
- Cameletti, M., Ignaccolo, R., Bande, S., 2011. Comparing spatio-temporal models for particulate matter in Piemonte. *Environmetrics* 22 (8), 985–996. <https://doi.org/10.1002/env.1139>.
- Cameletti, M., Lindgren, F., Simpson, D., Rue, H., 2013. Spatio-temporal modeling of particulate matter concentration through the SPDE approach. *AStA Adv Stat Anal* 97 (2), 109–131. <https://doi.org/10.1007/s10182-012-0196-3>.
- Cheam, A.S.M., Marbac, M., McNicholas, P.D., 2017. Model-based clustering for spatiotemporal data on air quality monitoring. *Environmetrics* 28 (3), e2437. <https://doi.org/10.1002/env.2437>.
- Chen, L., Guo, B., Huang, J., He, J., Wang, H., Zhang, S., Chen, S.X., 2018. Assessing air quality in Beijing-Tianjin-Hebei region: the method and mixed tales of PM<sub>2.5</sub> and O<sub>3</sub>. *Atmos. Environ.* 193, 290–301. <https://doi.org/10.1016/j.atmosenv.2018.08.047>.
- Cheng, J., Karambelkar, B., Xie, Y., 2019. Leaflet: Create Interactive Web Maps with the JavaScript ‘Leaflet’ Library. R package version 2.0.3. <https://CRAN.R-project.org/package=leaflet>.
- Clifford, S., Low-Choy, S., Mazaheri, M., Salimi, F., 2019. A Bayesian spatiotemporal model of panel design data: airborne particle number concentration in Brisbane, Australia. *Environmetrics* 30 (7), e2597. <https://doi.org/10.1002/env.2597>.
- Departament de Salut. Cartography [Available at: [https://salutweb.gencat.cat/ca/el\\_departament/estadistiques\\_sanitaries/cartografia/](https://salutweb.gencat.cat/ca/el_departament/estadistiques_sanitaries/cartografia/). (Accessed 27 February 2021). last accessed on.
- Fiovaranti, G., Martino, S., Cameletti, M., Cattani, G., 2021. Spatio-temporal modelling of PM<sub>10</sub> daily concentrations in Italy using the SPDE approach. *Atmos. Environ.* 248, 118192. <https://doi.org/10.1016/j.atmosenv.2021.118192>.
- Departament de Territori i Sostenibilitat. Generalitat de Catalunya [Available at: <https://analisi.transparenciacatalunya.cat/en/Medi-Ambient/Qualitat-de-l-aire-als-punts-de-mesurament-autom-t/tasf-thgu>. (Accessed 27 February 2021). last accessed on.
- Statistical Institute of Catalonia [Available at: Idescat <https://www.idescat.cat/?lang=en>. (Accessed 27 February 2021). last accessed on.
- Krainski, E.T., 2018. Statistical Analysis of Space-Time Data: New Models and Applications, vol. 93. Doctoral Thesis at NTNU.
- Krainski, E.T., Gómez-Rubio, V., Bakka, H., Lenzi, A., Castro-Camilo, D., Simpson, D., Lindgren, F., Rue, H., 2020. Advanced Spatial Modelling with Stochastic Partial Differential Equations Using R and INLA. Chapman and Hall/CRC, London (chapter 2).5 [Available at: <https://becarioprecario.bitbucket.io/spde-gitbook/>. (Accessed 6 March 2021). last accessed on.
- Liang, X., Zou, T., Guo, B., Li, S., Zhang, H., Zhang, S., Huang, H., Chen, S.X., 2015. Assessing Beijing’s PM<sub>2.5</sub> pollution: severity, weather impact, APEC and winter

- heating. *Proc R Soc A* 471 (2182), 20150257. <https://doi.org/10.1098/rspa.2015.0257>.
- Liang, X., Li, S., Zhang, S., Huang, H., Chen, S.X., 2016. PM<sub>2.5</sub> data reliability, consistency, and air quality assessment in five Chinese cities. *JCR Atmospheres* 121 (17), 10220–10236. <https://doi.org/10.1002/2016JC024877>.
- Lindgren, F., Rue, H., 2015. Bayesian spatial modelling with R-INLA. *J. Stat. Software* 63 (19). <https://doi.org/10.18637/jss.v063.i19>.
- Lindgren, F.K., Rue, H., Lindström, J., 2011. An explicit link between Gaussian fields and Gaussian Markov random fields: the stochastic partial differential equation approach. *J R Stat Soc Series B Stat Methodol* 73 (4), 423–498. <https://doi.org/10.1111/j.1467-9868.2011.00777.x>.
- Meteocat, Generalitat de Catalunya. Meteorological data from XEMA. Available at: <http://analisi.transparenciacatalunya.cat/en/Medi-Ambient/Dades-meteorol-giques-d-e-la-XEMA/nzvn-apee>. (Accessed 27 February 2021). last accessed on.
- Mukhopadhyay, S., Sahu, S.K., 2018. A Bayesian spatiotemporal model to estimate long-term exposure to outdoor air pollution at coarser administrative geographies in England and Wales. *J R Stat Soc Ser A-Stat Soc.* 181 (2), 465–486. <https://doi.org/10.1111/rssa.12299>.
- Nicolis, O., Díaz, M., Sahu, S.K., Marín, J.C., 2019. Bayesian spatiotemporal modeling for estimating short-term exposure to air pollution in Santiago de Chile. *Environmetrics* 30 (7), e2574. <https://doi.org/10.1002/env.2574>.
- Ossandón, A., Brunner, M.I., Rajagopalan, B., Kleiber, W., 2021. A space-time Bayesian hierarchical modeling framework for projection of seasonal streamflow extremes. *Hydrol. Earth Syst. Sci. Discuss.* 1–34. <https://doi.org/10.5194/hess-2021-270>.
- Pirani, M., Gulliver, J., Fuller, G.W., Blangiardo, M., 2013. Bayesian spatiotemporal modelling for the assessment of short-term exposure to particle pollution in urban areas. *J. Expo. Sci. Environ. Epidemiol.* 27, 1–9. <https://doi.org/10.1038/jes.2013.85>.
- R INLA project, 2021a. Random walk of order 1 (RW1) [Available at; last accessed on March 12, 2021]. <https://inla.r-inla-download.org/r-inla.org/doc/latent/rw1.pdf>.
- R INLA project, 2021b. Model for seasonal variation [Available at: <https://inla.r-inla-download.org/r-inla.org/doc/latent/seasonal.pdf>. (Accessed 12 March 2021). last accessed on.
- Version 2.18 [Available at: <https://qgis.org/downloads/>. (Accessed 27 February 2021). last accessed on.
- R INLA project, 2021c. Available at; last accessed on March 12, 2021]. <http://www.r-inla.org/home>.
- Richmond-Bryant, J., Long, T.C., 2020. Influence of exposure measurement errors on results from epidemiological studies of different designs. *J. Expo. Sci. Environ. Epidemiol.* 30, 420–429. <https://doi.org/10.1038/s41370-019-0164-z>.
- Rue, H., Martino, S., Chopin, N., 2009. Approximate Bayesian inference for latent Gaussian models using integrated nested Laplace approximations (with discussion). *J R Stat Soc Series B Stat Methodol* 71, 319–392. <https://doi.org/10.1111/j.1467-9868.2008.00700.x>.
- Rue, H., Riebler, A., Sørbye, H., Illian, J.B., Simpson, D.P., Lindgren, F.K., 2017. Bayesian computing with INLA: a review. *Annual Reviews of Statistics and its Applications* 4 (March), 395–421. [annurev-statistics-060116-054045](https://doi.org/10.1111/arsa.12299).
- Saez, M., Tobias, A., Barceló, M.A., 2020. Effects of long-term exposure to air pollutants on the spatial spread of COVID-19 in Catalonia, Spain. *Environ. Res.* 191, 110177. <https://doi.org/10.1016/j.envres.2020.110177>.
- Shaddick, G., Yan, H., Vienneau, D., 2013. A Bayesian hierarchical model for assessing the impact of human activity on nitrogen dioxide concentrations in Europe. *Environ. Ecol. Stat.* 20, 553–570. <https://doi.org/10.1007/s10651-012-0234-z>.
- Simpson, D.P., Rue, H., Martins, T.G., Riebler, A., Sørbye, S.H., 2017. Penalising model component complexity: a principled, practical approach to constructing priors (with discussion). *Stat. Sci.* 32 (1), 1–46. <https://doi.org/10.1214/16-STS576>.
- Verdin, A., Rajagopalan, B., Kleiber, W., Podestá, G., Bert, F., 2019. BayGEN: a Bayesian space-time stochastic weather generator. *Water Resour. Res.* 2900–2915. <https://doi.org/10.1029/2017WR022473>.
- Wan, Y., Xu, M., Huang, H., Chen, S.X., 2021. A spatio-temporal model for the analysis and prediction of fine particulate matter concentration in Beijing. *Environmetrics* 32 (1), e2648. <https://doi.org/10.1102/env.2648>.
- Wannemuehler, K., Lyles, R., Waller, L., Hoekstra, R., Klein, M., Tolbert, P., 2009. A conditional expectation approach for associating ambient air pollutant exposures with health outcomes. *Environmetrics* 20 (7), 877–894. <https://doi.org/10.1002/env.978>.
- Wright, N., Newell, K., Lam, K.B.H., Kurmi, O., Chen, Z., Kartsonaki, C., 2021. Estimating ambient air pollutant levels in Suzhou through the SPDE approach with R-INLA. *Int. J. Hyg Environ. Health* 235, 113766. <https://doi.org/10.1016/j.ijheh.2021.113766>.